Aerosol Behavior in Temperature and Concentration Gradient Fields in Nonisothermal Tube Flow

A general aerosol dynamics equation is derived for nonisothermal steady flow in cylindrical geometry. A scheme for the numerical solution of this equation is presented and its application is illustrated for a practical case incorporating condensation, nucleation, and thermophoresis effects. Additionally, the results of the numerical computations are compared with laboratory experimental measurements of changes in aerosol concentrations and size distributions for nonisothermal flow through a horizontal circular tube.

A. R. NADKARNI and R. MAHALINGAM

Department of Chemical Engineering
Washington State University
Pullman, WA 99164

SCOPE

Particulates are undesirable byproducts of combustion and gasification processes not only because of their environmental hazards, but because of their ability to stimulate chemical corrosion and mechanical erosion during processing. In view of the problems associated with the presence of particulates, accurate monitoring of aerosol streams is very desirable to enable the precise design of particulate control equipment. This necessitates the availability of a true picture of aerosol behavior in aerosol containment and transport systems. Another important potential application of this information is in aerosol flow reactors, in which aerosol dynamics plays a very important role in the reaction rates and conversions.

Aerosol behavior in a given flow situation can be completely represented through aerosol population balance considerations. In the present study the following phenomena are considered in the derivation of aerosol population balance equation for cylindrical geometry: particle coagulation; homogeneous nucleation and condensation of condensable vapors present in the stream; Brownian diffusion; sedimentation; and thermophoresis. A numerical solution of the resulting integro-differential equation is then developed for a typical industrial aerosol stream, for example, the off-gas stream from a coal gasifier bed. The decrease in partial pressure of the condensable vapors is taken into account by coupling the aerosol population balance with the mass balance on the condensable component. The temperature distribution within the pipe is obtained by solution of the energy balance equation. A finite difference numerical method is used in the solution of the above system of equations.

An experimental unit was constructed to generate and monitor an appropriate aerosol stream. The experiments consisted of measurements of changes in aerosol loadings and size distributions during the flow through a horizontal circular tube. Different substances were used to produce the aerosols, depending on their suitability at the temperatures employed. The experimental results are compared with corresponding numerical computations based on the model development. These results provide information on the relative magnitudes of the individual phenomena under varying experimental conditions.

CONCLUSIONS AND SIGNIFICANCE

From the solution of the general aerosol dynamics equations, like the one presented here for cylindrical geometry, it is possible to derive valuable information regarding aerosol behavior. The application discussed in this paper shows that from the data available at a reference point, it is possible to calculate aerosol loading and size distribution at any axial location in pipe flow. This has an important application in situations such as coal combustion and gasification, where accurate characterization of product gas streams is very important. For example, changes in particle loading and size distribution may take place as a sample is drawn from the gas lines through a sampling probe. The particle loading and size distribution recorded by analytical instruments at the end of the probe thus may not accurately represent the conditions at the sampling point, especially considering the magnitudes of temperature gradients set up as the sample stream is cooled from a main stream temperature of about 1,000 K to a temperature close to ambient. Analysis of particle dynamics enables us to predict these changes. The studies here show that particulate losses as high as 80% could occur under certain conditions in horizontal pipe flow, the number loss being lower than mass loss for the size ranges studied. Performance of aerosol reactors is intimately linked to the aerosol behavior, hence this study is directly applicable to the modeling of aerosol flow reactors. Solution of the dynamic equation also provides us with a tool for the mathematical evaluation of the contribution of each process, such as Brownian diffusion, coagulation, etc., in the overall aerosol behavior.

In this paper we have also illustrated an experimental arrangement for the generation and monitoring of aerosol streams. Comparisons of experimental measurements with theoretical predictions show good agreement, which confirms the validity of the numerical solutions. By comparing the data obtained at

Correspondence concerning this paper should be addressed to R. Mahalingam.

different experimental conditions such as flow rate, temperature gradient, and aerosol loading, we are able to analyze the relative magnitudes of various processes. Examination of experimental and numerical results shows that thermophoresis is the most important factor under the experimental conditions. This underlines the important role played by temperature gradients in aerosol dynamics.

BACKGROUND

Particles suspended in a gas—the gas being either confined in an enclosed space or flowing in a conduit or through equipment—are in a state of constant motion. Apart from the bulk gas motion, some of the other forces which keep the particles in motion are Brownian diffusion under a particle concentration gradient, sedimentation under gravity, thermophoresis under temperature gradient, and diffusiophoresis under a gas concentration gradient in a binary or multicomponent gas mixture. The particle motion generates a change in bulk and local loading and in size distribution. This is because the diffusive, gravitational and thermophoretic forces are size-dependent; hence particle deposition at the walls of the container or the pipe is different for different sizes. Other processes responsible for changes in size distribution are coagulation and condensation. Due to the random Brownian motion, particles collide with each other. The colliding particles adhere or coalesce to form larger particles. If the gas contains saturated vapor, nucleation occurs to generate entirely new particles and condensation occurs on the existing particles to enable the particles to grow.

In one of the first attempts to study the combined effect of two or more aerosol transport processes, Gormley and Kennedy (1949) developed an analytical expression for diffusion from a stream flowing in a circular tube. DeMarcus and Thomas (1952) obtained similar expressions for a parallel-sided channel. Further improvements included the addition of a formation term by Berezhnoi and Kirichenko (1964), axial diffusion term by Tan and Hsu (1971), and the effect of entrance region by Hsu (1967). Moo-Young and Yamaguchi (1975) studied the combined effect of thermophoresis and settling in a flow between two parallel plates. In more recent important studies related to aerosol dynamics, Gelbard and Seinfeld (1979) obtained an analytical solution for the dynamic equation for an aerosol confined in a closed space and undergoing growth by coagulation, condensation, and nucleation. Crump and Seinfeld (1980) considered flow in a continuous stirred tank reactor (CSTR) with coagulation, condensation, and nucleation. Damle and Mahalingam (1982) studied aerosol behavior in a spherical geometry with changes taking place due to coagulation, sedimentation, and Brownian diffusion. In the case of aerosol behavior in a pipe flow, the problem of particular interest is the effect of temperature gradient fields, which often occur in industrial gas-aerosol systems but which seem to have attracted little attention despite their role in governing the rates of condensation, nucleation, and thermophoresis. This problem has been investigated in detail, as described below. This has been extended by Nguyen and Mahalingam (1982) to temperature effects in a CSTR; the method of solution, however, is different.

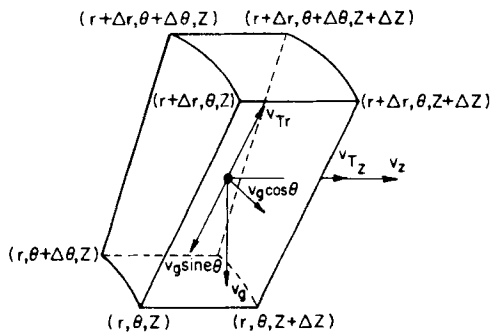

Figure 1. Volume element in cylindrical geometry.

EQUATIONS DESCRIBING AEROSOL BEHAVIOR IN PIPE FLOW

Consider steady flow of an aerosol stream in a circular pipe. The carrier gas stream is composed of a noncondensable gas and the condensable vapors of the single component forming the aerosol. Assume that the following conditions are known at the pipe inlet: (i) particle size distribution and loading; (ii) temperature of the stream; (iii) partial pressure of the condensable vapors. The following equaitons will then describe the aerosol behavior in the pipe flow.

Aerosol Population Balance Equation

The aerosol population balance equation is derived by formulating the time rate of change in number density in a differential volume element due to each of the following processes and equating the net rate to zero under steady state conditions:

(a) Bulk flow
(b) Brownian diffusion of the aerosol under radial and axial particle concentration gradients
(c) Gravitational settling
(d) Thermophoresis under radial and axial temperature gradients
(e) Condensation of vapors on the aerosol particles
(f) Homogeneous nucleation of the condensable vapors
(g) Coagulation or coalescence of particles to form larger particles

Consider a volume element in cylindrical geometry (Figure 1) at position (r,θ,z), of radial dimension Δr, axial dimension Δz, and subscribing an angle $\Delta\theta$ at the centerline. Let $n(r,\theta,z,d)$ represent the number density of particles of diameter d at (r,θ,z). The rate of change in number density, $\dot{n}$, due to each of the above processes is obtained below.

Bulk Flow in Axial Direction.

$$\dot{n}_{\text{bulk flow}} = -v_z \frac{\partial n}{\partial z} \tag{1}$$

Brownian Diffusion. Particles diffuse in the direction of a decreasing particle concentration gradient. A radial concentration gradient is established due to zero concentration at the pipe wall, giving rise to an outward radial diffusion of particles. Also, due to deposition at the wall, particle concentration diminishes axially. The axial concentration gradient is usually very small, hence the axial diffusion is neglected. The rate of change in number density due to radial particle diffusion is given by

$$\dot{n}_{\text{diffusion}} = D_p \left\{ \frac{1}{r} \frac{\partial}{\partial r} \left(r \frac{\partial n}{\partial r} \right) \right\} \tag{2}$$

For particles of diameter smaller than the gas mean free path, the particle diffusivity in the carrier gas is given by Langmuir's equation.

$$D_p = \frac{4kT}{3\pi d^2 P} \left(\frac{8R_g T}{\pi m} \right)^{1/2} \tag{3}$$

For particles of diameter larger than the gas mean free path, it is given by Einstein's equation.

$$D_p = \frac{C_d kT}{3\pi\mu d} \tag{4}$$

The Cunningham correction factor for a particle of diameter d is given by

$$C_d = 1 + \frac{2\lambda}{d}\left\{1.257 + 0.4\exp\left(\frac{-0.55d}{\lambda}\right)\right\} \quad (5)$$

where λ, the gas mean free path, is obtained from kinetic theory.

$$\lambda = \frac{\mu}{0.499\rho\bar{u}} \quad (6)$$

Gravitational Settling. In a horizontal pipe,

$$\dot{n}_{\text{sedimentation}} = \frac{v_g \sin\theta}{r}\frac{\partial}{\partial r}(nr) + \frac{v_g}{r}\frac{\partial}{\partial\theta}(n\cos\theta) \quad (7)$$

In a vertical pipe,

$$\dot{n}_{\text{sedimentation}} = v_g\frac{\partial n}{\partial z} \quad (8$$

The terminal settling velocity is given by Stokes' law.

$$v_g = \frac{\rho_p d^2 g C_d}{18} \quad (9)$$

Thermophoresis. A particle in a temperature gradient field is subjected to thermophoresis. Gas molecules striking the side of the particle facing the high temperature region have more kinetic energy on an average than those hitting on the low temperature side. Pilat and Prem (1976) have reported the following expressions for thermophoretic velocity, v_T. For particles of diameter less than the gas mean free path, it is given by

$$v_T = \frac{-15\pi\bar{u}\lambda}{16(8+\pi a_c)T}\nabla T \quad (10)$$

For particles of diameter greater than the gas mean free path,

$$v_T = \frac{-3\mu}{\rho T}\cdot\frac{(K + 2.16K_pKn)\nabla T}{(2K + K_p + 4.32K_pKn)(1 + 2.26Kn)} \quad (11)$$

The following rate expressions are obtained based on radial and axial components of thermophoretic velocity:

$$\dot{n}_{\text{radial thermophoresis}} = -\frac{1}{r}\cdot\frac{\partial}{\partial r}(v_{Tr}\cdot r\cdot n) \quad (12)$$

$$\dot{n}_{\text{axial thermophoresis}} = -\frac{\partial}{\partial z}(v_{Tz}\cdot n) \quad (13)$$

Condensation. The driving force for condensation is the difference between vapor concentration in the bulk and that on the particle surface. This concentration gradient causes the diffusion of condensable vapors to the particle surface where they condense, resulting in particle growth. Particle growth by condensation is controlled by the rate of diffusion of condensable vapors. Hidy and Brock (1970) have reported the following expressions for condensation growth rate of particles of diameter d:

$$I(p,T,d) = \frac{dd}{dt} = \frac{4D_vM_p}{R_gTd\rho_p}(p - p') \quad (14)$$

The net rate of formation of particles of diameter d due to condensation can be obtained as

$$\dot{n}_{\text{condensation}} = -I(p,T,d)\frac{\partial n}{\partial d} \quad (15)$$

Homogeneous Nucleation. Depending on the degree of supersaturation, spontaneous condensation—called nucleation—is observed. The rate of change in number density of particles of diameter d due to nucleation is given by

$$\dot{n}_{\text{nucleation}} = S_o(p,T)\cdot\delta(d - d_o) \quad (16)$$

Hidy and Brock (1970) have reported the following expressions for the rate of nucleation and the size of the nuclei.

$$S_o = \frac{\alpha_c p\pi d^2 n_v}{(2\pi m_v kT)^{1/2}}\exp\left(-\frac{\Delta G_o}{kT}\right) \quad (17)$$

$$d_o = \frac{4\sigma V_L}{kT\ln\left(\frac{p}{p'}\right)} \quad (18)$$

When the vapor becomes supersaturated, the free energy of formation of the embryo displays a maximum value ΔG_o at the embryo diameter d_o. When partial pressure p is greater than vapor pressure p', droplet embryos of diameter d_o are unstable and tend to disappear, whereas droplet embryos of diameters greater than d_o tend to grow. The free energy of formation of the critical size embryo is given by

$$\Delta G_o = \frac{\pi d_o^2\sigma}{3} \quad (19)$$

Coagulation. The net rate of change in concentration of particles of diameter d due to coagulation is the difference between the term representing the generation of particles of diameter d due to collision of smaller particles, and the term representing the loss of particles of diameter d due to their collisions with other particles.

$$\dot{n}_{\text{coagulation}} = \int_0^{d/2^{1/3}} \beta\{(d^3 - \bar{d}^3)^{1/3},\ \bar{d}\} \cdot n\{(d^3 - \bar{d}^3)^{1/3}\}n(\bar{d})d\bar{d} - \int_0^{\infty}\beta(d,\bar{d})\cdot n(d)n(\bar{d})d\bar{d} \quad (20)$$

The collision coefficient for a pair of particles with sizes d_1 and d_2 is given by Smoluchowski's equation.

$$\beta(d_1,d_2) = \frac{2kT}{3\mu}(d_1 + d_2)\left[\frac{C_{d_1}}{d_1} + \frac{C_{d_2}}{d_2}\right] \quad (21)$$

Final Equation and Boundary Conditions

In a steady state system the net rate of change in number density is zero. The final aerosol population balance equation is thus obtained by summing the various contributions to change in number density of particles of diameter d, and equating the sum to zero.

$$-v_z\frac{\partial n}{\partial z} + D_p\left\{\frac{1}{r}\frac{\partial}{\partial r}\left(r\frac{\partial n}{\partial r}\right)\right\} + \frac{v_g\sin\theta}{r}\frac{\partial}{\partial r}(nr) + \frac{v_g}{r}\frac{\partial}{\partial\theta}(n\cos\theta) - \frac{1}{r}\frac{\partial}{\partial r}(rv_{Tr}n) - \frac{\partial}{\partial z}(v_{Tz}n) - I(p,T,d)\frac{\partial n}{\partial d} + S_o(p,T)\delta(d - d_o) + \int_0^{d/2^{1/3}}\beta\{(d^3 - \bar{d}^3)^{1/3},\bar{d}\}n\{(d^3 - \bar{d}^3)^{1/3}\}\cdot n(\bar{d})d\bar{d} - \int_0^{\infty}\beta(d,\bar{d})n(d)n(\bar{d})d\bar{d} \quad (22)$$

Equation 22 is written for a horizontal pipe. Solution of this equation requires four boundary conditions as follows.

(i) Size distribution of entering aerosol is uniform and is known (i = inlet)

$$n(r,\theta,0,d) = n_i(d) \quad (23)$$

(ii) Concentration of particles on the pipe wall is assumed to be zero; i.e., a particle is assumed to lose its identity and become a part of the wall as soon as it is deposited at the wall (r_i = inside radius)

$$n(r_i,\theta,z,d) = 0 \quad (24)$$

(iii) Based on the continuity of concentration profile at the axis

$$\left(\frac{\partial n}{\partial r}\right)_{0,\theta,z,d} = -\left(\frac{\partial n}{\partial r}\right)_{0,\theta+\pi,z,d} \quad (25)$$

(iv) Symmetry with respect to the vertical centerline of the circular cross section gives

$$\left(\frac{\partial n}{\partial\theta}\right)_{r,\pi/2,z,d} = \left(\frac{\partial n}{\partial\theta}\right)_{r,3\pi/2,z,d} = 0 \quad (26)$$

In the case of an upward vertical flow, the sedimentation term in Eq. 22 is replaced by the expression given in Eq. 8. In this case, n is a function of only r and z, hence only three boundary conditions are required as given in Eqs. 23, 24, and 25.

TEMPERATURE DISTRIBUTION

As the stream flows in the pipe, axial and radial temperature gradients are established due to heat loss through the pipe wall. The temperature profile is obtained by solution of the steady state equation of energy:

$$-v_z\frac{\partial T}{\partial z}+\alpha\left\{\frac{1}{r}\frac{\partial}{\partial r}\left(r\frac{\partial T}{\partial r}\right)\right\}=0 \tag{27}$$

The axial conduction term is small in comparison to the axial convective transport term and the radial conduction term, hence it is ignored. Also, since the condensable vapors constitute a very small fraction of the stream, the heat effects involved in the condensation process are ignored. The solution of Eq. 27 requires three boundary conditions:

(i) $T(r,0)=T_i$ (28)

(ii) $\left(\frac{\partial T}{\partial r}\right)_{0,z}=0$ (29)

(iii) Two wall boundary conditions of practical importance:

Constant wall temperature

$$T(r_t,z)=Tw \tag{30a}$$

Constant wall heat flux

$$K\left(\frac{\partial T}{\partial r}\right)_{r_t,z}=-q \tag{30b}$$

CONDENSABLE COMPONENT MASS BALANCE

The rates of the condensation and nucleation processes at any point depend on the existing partial pressure of the condensable vapor. At the same time, the partial pressure of the condensable vapor depends on the total loss of material from the vapor phase due to condensation and nucleation. The partial pressure distribution for the condensable vapor is obtained by simultaneous solution of the aerosol population balance equation and the condensable component mass balance which is given below.

$$-v_z\frac{dp}{dz}=\frac{\pi R_g T\rho_p}{M}\int_0^\infty\left\{I(p,T,d)d^2\cdot n+\frac{S_o(p,T)}{6}d_o^3\right\}dd \tag{31}$$

Only one boundary condition needs to be specified

$$p=p_i \text{ at } z=0 \text{ for all } r \text{ and } \theta \tag{32}$$

NONDIMENSIONALIZATION OF EQUATIONS

Equations 22, 27, and 31 are nondimensionalized by defining the following dimensionless variables.

$$R=\frac{r}{r_t},\quad Z=\frac{z}{r_t},\quad D=\frac{d}{d_{\text{mean}}}$$

$$\tau=\frac{T}{T_i},\quad N=\frac{n}{N_o},\quad P=\frac{p}{p_i}$$

$$VZ=\frac{v_z}{\bar{v}_z},\quad VG=\frac{v_g}{\bar{v}_z},\quad VTR=\frac{v_{Tr}}{\bar{v}_z},\quad VTZ=\frac{v_{Tz}}{\bar{v}_z}$$

$$Pr=\frac{C\mu}{K},\quad Re=\frac{2\bar{v}_z r_t\rho}{\mu},\quad Pe=\frac{D_p}{2\bar{v}_z r_t}$$

$$\Omega=\frac{gr_t}{KT_i},\quad \Psi=\frac{I}{\bar{v}_z\left(\frac{d_{\text{mean}}}{r_t}\right)},\quad \Phi=\frac{S_o r_t}{\bar{v}_z N_o}$$

$$BK=\frac{\beta_o r_t}{\bar{v}_z N_o},\quad B=\frac{\beta}{\beta_o}$$

Aerosol Population Balance

$$-VZ\frac{\partial N}{\partial Z}+2Pe\left(\frac{\partial^2 N}{\partial R^2}+\frac{1}{R}\frac{\partial N}{\partial R}\right)+VG\sin\theta\frac{\partial N}{\partial R}+\frac{VG\cos\theta}{R}\frac{\partial N}{\partial\theta}-\left(VTR\frac{\partial N}{\partial R}+VTR\cdot\frac{N}{R}+N\frac{\partial(VTR)}{\partial R}\right)$$
$$-VTZ\frac{\partial N}{\partial Z}-\Psi(P,\tau,D)\cdot\frac{\partial N}{\partial D}+\Phi(P,\tau)\delta(D-D_o)+BK\int_0^{D/2^{1/3}}B\{(D^3-\bar{D}^3)^{1/3},\bar{D}\}N\{D^3-\bar{D}^3)^{1/3}\}\cdot N(\bar{D})\cdot d\bar{D}-BK\int_0^\infty B(D,\bar{D})N(D)\cdot N(\bar{D})\cdot d\bar{D}=0 \tag{33}$$

Boundary Conditions

$$N(R,\theta,0,D)=N_i(D) \tag{34}$$

$$N(1,\theta,Z,D)=0 \tag{35}$$

$$\left(\frac{\partial N}{\partial R}\right)_{0,\theta,Z,D}=-\left(\frac{\partial N}{\partial R}\right)_{0,\theta+\pi,Z,D} \tag{36}$$

Energy Balance

$$-VZ\frac{\partial\tau}{\partial Z}+\frac{2}{Pr\cdot Re}\left(\frac{\partial^2\tau}{\partial R^2}+\frac{1}{R}\frac{\partial\tau}{\partial R}\right)=0 \tag{37}$$

Boundary Conditions

$$\tau(R,0)=0 \tag{38}$$

$$\left(\frac{\partial\tau}{\partial R}\right)_{0,Z}=0 \tag{39}$$

$$\tau(1,Z)=\tau_w, \text{ or} \tag{40}$$

$$\left(\frac{\partial\tau}{\partial R}\right)_{1,Z}=-\Omega \tag{41}$$

Condensed Component Mass Balance

$$-VZ\frac{\partial P}{\partial Z}=\left(\frac{W_p}{\rho_v}\right)\tau\times\int_0^\infty[6\psi(P,\tau,D)\cdot D^3\cdot N(D)+\Phi D_o^3]dD \tag{42}$$

W_p is the mass concentration of particles in the entering stream when all particles are of uniform size,

$$W_p=\frac{\pi}{6}d_{\text{mean}}^3 N_o\rho_p \tag{43}$$

Boundary Condition

$$P(R,\theta,0)=1 \tag{44}$$

NUMERICAL SOLUTION

A computer code was developed (Nadkarni, 1982) for the solution of the above equations using an implicit finite difference method. This program is based on the following major simplifications.

(i) Typically, the aerosol particles and vapors constitute only a very small fraction of the stream, hence stream properties are approximated by those of the noncondensable gas.

TABLE 1. OFF-GAS STREAM FROM A COAL GASIFIER (NADKARNI, 1982)

Pipe orientation: horizontal
Aerosol density at inlet = 10^6 particles/m^3
Inlet size distribution: log normal
  No. of particle sizes = 10
  Min. particle dia. = 0.2 μm
  Max. particle dia. = 20.0 μm
  Std. deviation = 1.8
Inlet temperature: 800 K
Wall temperature: 298 K
Total pressure: 9.2×10^5 N/m^2
Molar mass of carrier gas: 24.5 kg/kmol
Specific heat: $1{,}201.8 + 0.0235T$ J/kg·K
Thermal conductivity (273 K): 0.045 W/m·K
Viscosity (273 K): 1.4×10^{-5} kg/m·s
Properties of condensable vapor and liquid particles
  Molecular mass: 185 kg/kmol
  Inlet particle pressure: 0.02×10^{-5} N/m^2
  Surface tension (273 K): 0.031 N/m
  Diffusivity of vapor in carrier gas (273 K): 1.0×10^{-5} m^2/s
  Vapor pressure: $P' = 10^5 \exp\left(11.94 - \frac{7{,}494}{T + 14.75}\right)$ N/m^2

(ii) Particle size distribution is assumed to be discrete in character (in view of the experimental measurements being so). A range of discrete particle sizes is specified in the input data, and each particle is assumed to exist in only one of these sizes.

(iii) The program is designed to handle the following possible flow regimes: fully developed laminar flow; fully developed turbulent flow; and undeveloped flow in the pipe entrance region. Exact expressions for point axial velocity are known for laminar flow and for flow in the entrance region (Langhaar, 1942). For turbulent flow, however, the calculations are based on time-averaged velocity as given by the Blasius equation. The fluctuating component of the turbulent flow and its consequences on aerosol dynamics are ignored.

The algorithm for numerical solution has six steps.

1. Uniform grid temperatures are assumed in the initial guess, which are then corrected by direct substitution iterations until a converged solution is obtained. The stream properties at each point are corrected for local temperature during each iteration.

2. Based on the assumed size distribution and aerosol density, the coagulation term is evaluated. In the finite difference formulation, the integral is replaced by a summation over all particle sizes.

3. The partial pressure of the condensable vapors is evaluated in two steps as follows. In the finite difference form, Eq. 42 can be written as

$$-\frac{dp}{dZ} = C_1(P - P') + \frac{C_2}{\left(\ln \frac{P}{P'}\right)^2} \exp\left[\frac{-C_3}{\left(\ln \frac{P}{P'}\right)^2}\right] \tag{45}$$

Constants C_1, C_2, and C_3 depend, in addition to the physical properties of aerosol and carrier gas, also on the assumed particle loading and size distribution. Noting that the rate of nucleation is usually very small in comparison to the rate of condensation, Eq. 45 can be simplified to

$$-\frac{dP}{dZ} = C_1(P - P') \tag{46}$$

Solution of Eq. 46 is

$$P(R,\theta,Z) = P'(R,Z) + [1 - P'(R,1)] \cdot \left[\frac{1 - \exp(-C_1\Delta Z)}{C_1\Delta Z}\right]^{Z/\Delta Z} \tag{47}$$

Using this value of P on the righthand side of Eq. 45, a new value of P is numerically calculated. Usually the corrected value is fairly close to the assumed value, making additional iterations unnecessary.

4. The rates of condensation and nucleation are calculated on the partial pressure calculated in step 3.

5. Using the rates of coagulation, condensation, and nucleation calculated in steps 2 and 4, Eq. 33 is solved for each particle size to obtain new values for the number densities. If the calculated particle densities are not in agreement with assumed values, steps 2 to 5 are repeated. Normally, it is necessary to overrelax the calculated values before using them in the new guess.

6. Having obtained the converged solution, the fractional number penetration of particles of diameter D at axial position L is obtained from the following expression by numerical integration.

$$F(L,D) = \frac{\int_0^{2\pi} \int_0^1 N(R,\theta,L,D) R dR d\theta}{2\pi N_i(D)} \tag{48}$$

$$\text{Fractional deposition} = 1 - F(L,D) \tag{49}$$

The overall fractional number penetration is calculated from

$$FN(L) = \frac{1}{2\pi} \sum_{d_{min}}^{d_{max}} \int_0^{2\pi} \int_0^1 N(R,\theta,L,D) R dR d\theta \tag{50}$$

and the overall fractional mass penetration from

$$FM(L) = \frac{\sum_{d_{min}}^{d_{max}} \left[\int_0^{2\pi} \int_0^1 N(R,\theta,L,D) R dR d\theta\right] \cdot D^3}{2\pi \sum_{d_{min}}^{d_{max}} N_i(D) D^3} \tag{51}$$

COAL GASIFIER OFF-GAS STREAM EVALUATIONS

Nadkarni (1982) has illustrated the application of the above algorithm in the calculation of changes in aerosol density and size distribution in the flow of a coal gasifier product gas stream through a sampling probe. Some results of these calculations are shown in Figures 2 through 11. The data used in these calculations is given in Table 1.

Figure 2 shows the number size distribution of particles at different axial locations in laminar flow of gas. The size distribution

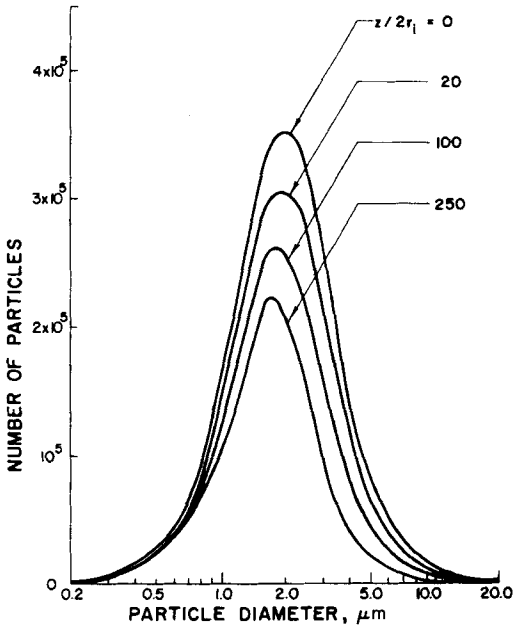

Figure 2. Number size distribution: horizontal pipe, fully developed laminar flow; *Re* = 1,200.

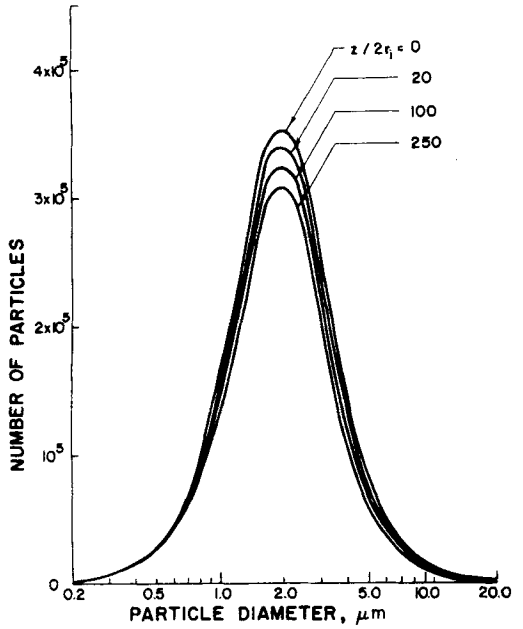

Figure 3. Number size distribution: horizontal pipe, turbulent flow; *Re* = 7,200.

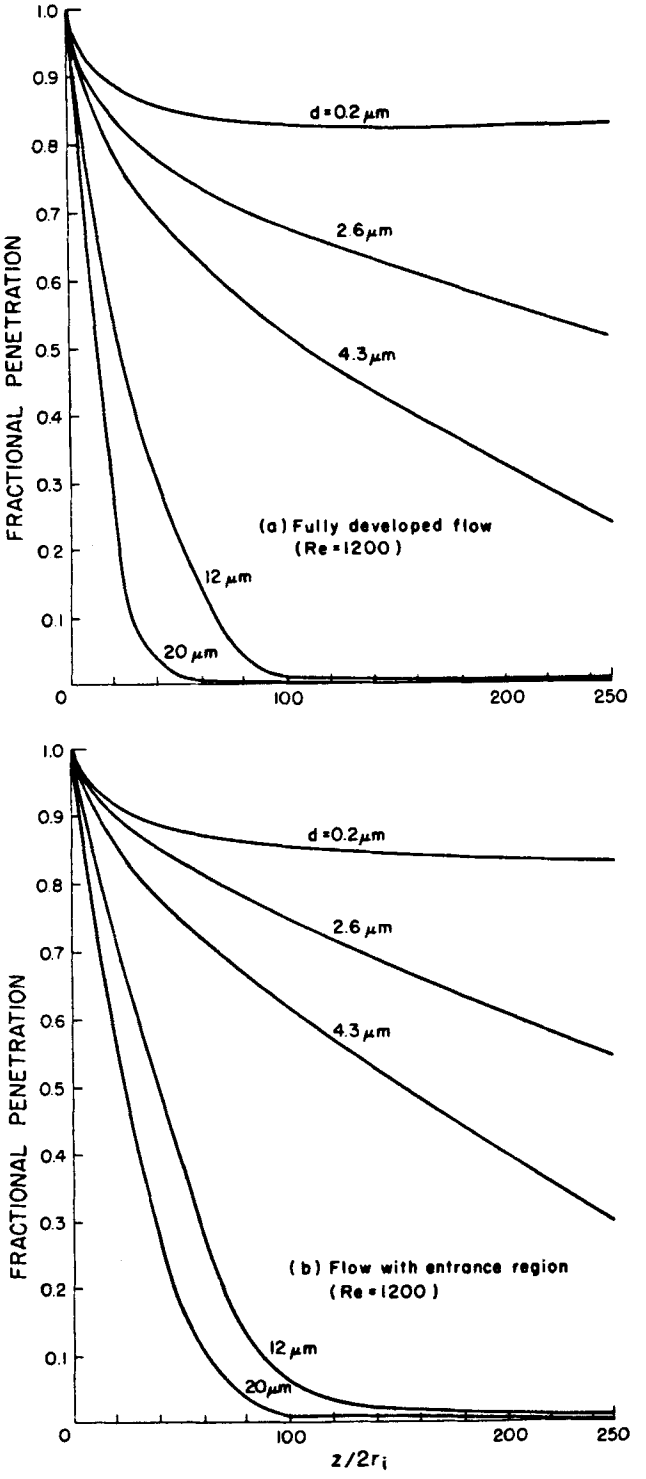

Figure 4. Number fractional penetration: horizontal pipe, laminar flow; *Re* = 1,200.

mean is shifted to the left with increasing distance from the inlet, indicating that the bigger particles deposit to a greater extent than the finer particles. This shift is less noticeable in turbulent flow (Figure 3), since particle deposition is less at higher gas velocities and convective transport is predominant.

Figure 4 shows the fractional penetrations of different particle sizes plotted against axial lengths in fully-developed laminar flow and in laminar flow with entrance region. The penetration of particles decreases as the size increases. This indicates that the combined effect of the forces responsible for particle deposition at the wall increases as the particle size increases. Since the Brownian diffusion is greater in smaller particles, this result also proves that the diffusive mechanism of deposition is small in comparison to thermophoretic and sedimentive deposition under the specified conditions. Figure 5 shows the penetrations for turbulent flow.

The overall fractional number penetration and mass penetration for the three types of flow are plotted in Figure 6. Note that the mass penetration is lower than the number penetration. The reason is that most of the aerosol mass is due to the larger particles which deposit to a greater extent than smaller particles.

Figure 7 shows the concentration profiles for 2.6 μm diameter particles, at pipe cross sections at different axial locations. The most notable feature of these concentration profiles is their dissymmetry with respect to the horizontal centerline of the circular cross section. This dissymmetry is due to the presence of a downward settling motion; it is more apparent in larger particles for which settling velocity is greater, and plays an important role in particle deposition (Figure 8). This dissymmetry is not pronounced in finer particles (Figure 9).

EXPERIMENTAL PROGRAM

The two broad objectives of the experimental work were:

(i) To measure the changes in concentration and size distribution of the aerosol stream during its flow through the tubular test section; and,

(ii) To compare the results from (i) above with theoretical predictions to confirm the applicability of the previously developed equations.

Experimental Setup

The experimental unit, shown schematically in Figure 10, consists of three sections: (i) aerosol generation section; (ii) test section; (iii) sampling assembly.

Aerosol Generation Section. A Constant Output Atomizer, TSI model 3076, is used to generate an aerosol stream. Pure nitrogen is used as the carrier gas in most of the high temperature experiments, while compressed air is used in the room temperature experiments. Compressed nitrogen from a cylinder or compressed air is filtered, dried, and then split into two streams. The dilution stream flow rate is measured by rotameter R_1 and the atomization stream flow rate is measured by rotameter R_2. The two flow rates are adjusted to obtain the desired aerosol concentration. The aerosol stream is combined with the dilution stream before it is led into the mixing chamber. The mixing chamber is a vertical cylindrical stainless steel vessel of 0.102 m ID and 0.457 m height (4 in. ID × 1.5 ft. height). The gas-aerosol mixture enters the vessel through a tangential inlet which ensures a vortex flow and a thorough mixing of dilution gas and aerosol. It also serves to remove larger droplets by impaction on the wall. At the outlet of the mixing chamber, a portion of the stream is purged and the desired portion is led

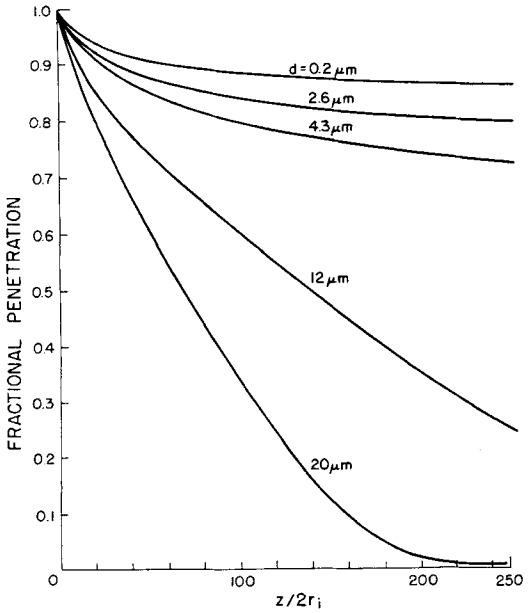

Figure 5. Number fractional penetration: horizontal pipe, turbulent flow; *Re* = 7,200.

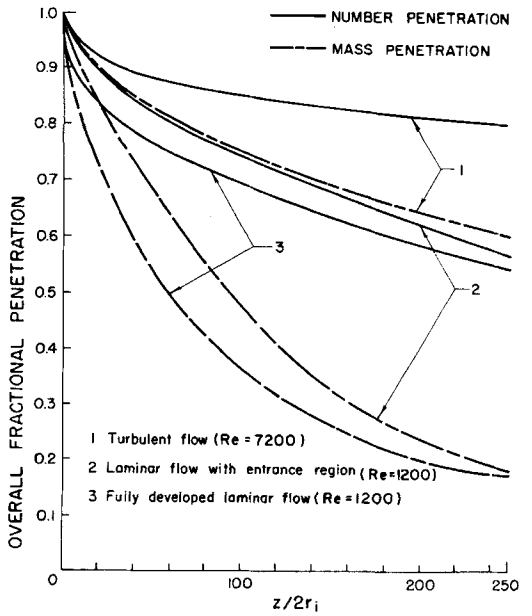

Figure 6. Overall fraction penetration.

to a charge neutralizer and on to the test section. A needle valve is used on the purge line for accurate control of the flow rate through the test section. To eliminate the influence of electrostatic charges created in the atomization process on the particle dynamics, the stream is sent through an Aerosol Charge Neutralizer, TSI model 3012. Before entering the test section, the stream is led through two cyclones having approximate cut points of 1.2 μm each.

Test Section. A 0.0095 m OD, 0.0077 m ID, and 2.13 m long ($\frac{3}{8}$ in. × 0.305 in. × 7 ft), horizontal stainless steel tube is used as the test section. Tappings in the form of tee connections are provided at either end of the tube for sampling the aerosol stream. Two thermocouples, one near the inlet and the other near the outlet, are used to measure the stream temperature at the two ends. The stream pressure at the inlet is indicated by a pressure gauge. Rotameter R_3 is used to measure the total flow through the test section minus the sampling flow.

Sampling Assembly. A parallel branch sampling unit is assembled to measure the concentration and size distribution of the aerosol sample. This assembly can be connected to either end of the test section. A different instrument is used on every branch. Each branch is provided with isolating ball valves, so that only one instrument can be used on line at any time. A GAST $\frac{1}{3}$ HP vacuum pump is used to draw the sample through the sampling assembly. Rotameter R_4 is used to measure the sample flow rate. Monitoring instruments used on the sampling assembly consists of filter papers, cascade impactor, diffusion battery, and electrical aerosol analyzer. Nuclepore polyester 0.2 μm and Gelman Teflon membrane 0.2 μm filter papers are used. A 47 mm stainless steel filter holder, Gelman model 2220, is used to secure the filter paper in line. Two types of cascade impactors, University of Washington Mark III and Sierra model 2210-K, are used. The impactor is enclosed in a cylindrical heating mantle to compensate for heat losses to the ambient from the sampling stream. Thermocouple junctions are cemented on the surfaces of the filter holder and impactor shell to monitor the temperature while sampling. An Electrical Aerosol Analyzer, TSI model 3030, is used for measurements in the submicron range, under room-temperature conditions.

Parts of the tubing before the test section, the cyclones, and all branches of the sampling assembly are wrapped with heavy insulated heating tapes to achieve the desired temperatures and to ensure that sampling is done at the same temperature as that of the main stream. The temperatures are controlled by regulating the voltage with three autotransformers and recorded on a 24-point Esterline Angus Multipoint Recorder. All the weighings are done on a Perkin-Elmer AD-2Z balance.

Experimental Results

The experimental program was carried out in two stages. In the first stage, the objective was limited to establishing the operability of the experimental setup at room temperature, using aqueous 0.2% methylene blue aerosol. The results (not shown here) showed good agreement in aerosol concentration measurements with filter paper, UW Mark III cascade impactor, and Sierra cascade impactor. The size distribution obtained from the electrical aerosol analyzer (EAA), however, showed disagreement with those measured using cascade impactors, particularly in the size range greater than 0.3 μm. One possible explanation is the constraint on the largest measureable size (0.75 μm) with the EAA.

The objective in the second stage of experimental work was to study the effects of flow rate, aerosol concentration, and temperature gradients. Test section inlet temperatures were varied from room temperature to 513 K. Three aerosol flow rates—83.3×10^{-6}, 136.7×10^{-6}, 333.3×10^{-6} m^3/s (std. cond.)—and two atomization-to-dilution ratios—1:7 and 1:0—were used. Altogether 34 experimental runs were carried out using dioctyl phthalate (DOP) (12 runs), propylene glycol (18 runs), and Therminol-60 (4 runs) as aerosol substances, based on their suitability (vapor pressure ranges) at the temperatures employed. Each experimental run consisted of measurements of aerosol loading and size distribution at the test section inlet and outlet. Each measurement with the cascade impactor was repeated using filter paper collection to confirm reproducibility and to eliminate errors. In all high-temperature runs, the test section wall was maintained at room temperature by circulating air through the concentric pipe jacketing the test section.

A detailed description of the experimental procedure and results of all experimental runs are reported by Nadkarni (1982). The results of four representative runs with propylene glycol are presented here. In Figures 11a through 11d, the solid curve represents the aerosol size distribution at the test section outlet measured experimentally using the UW Mark III cascade impactor. The broken curve represents the theoretical calculation of the size distribution at the outlet, based on experimental measurements of the distribution at the inlet. The fractional penetrations measured experimentally with cascade impactor and filter paper, and calculated theoretically, based on the mathematical analyses presented in the previous section, are also indicated in each figure.

DISCUSSION OF EXPERIMENTAL RESULTS

Figures 11a and 11b represent the size distribution and fractional penetration data for propylene glycol aerosol at the same flow rate (83.3×10^{-6} m^3/s) and same temperature gradient, but at different aerosol densities as produced by different atomization-to-dilution stream ratios. Comparison of these figures shows that the aerosol density does not have any observable effect on fractional penetration or on size distribution. The small differences do not show any specific trend and are within the range of experimental error. Based on theoretical analyses, however, at higher particle concentrations the coagulation process is enhanced, resulting in a greater number of larger particles and hence in a greater deposition or less penetration. The conclusion is, therefore, that the coagulation process has very little effect compared to the bulk stream motion and other processes. Hence the changes are not observable over the length of the test section used in the laboratory experiments.

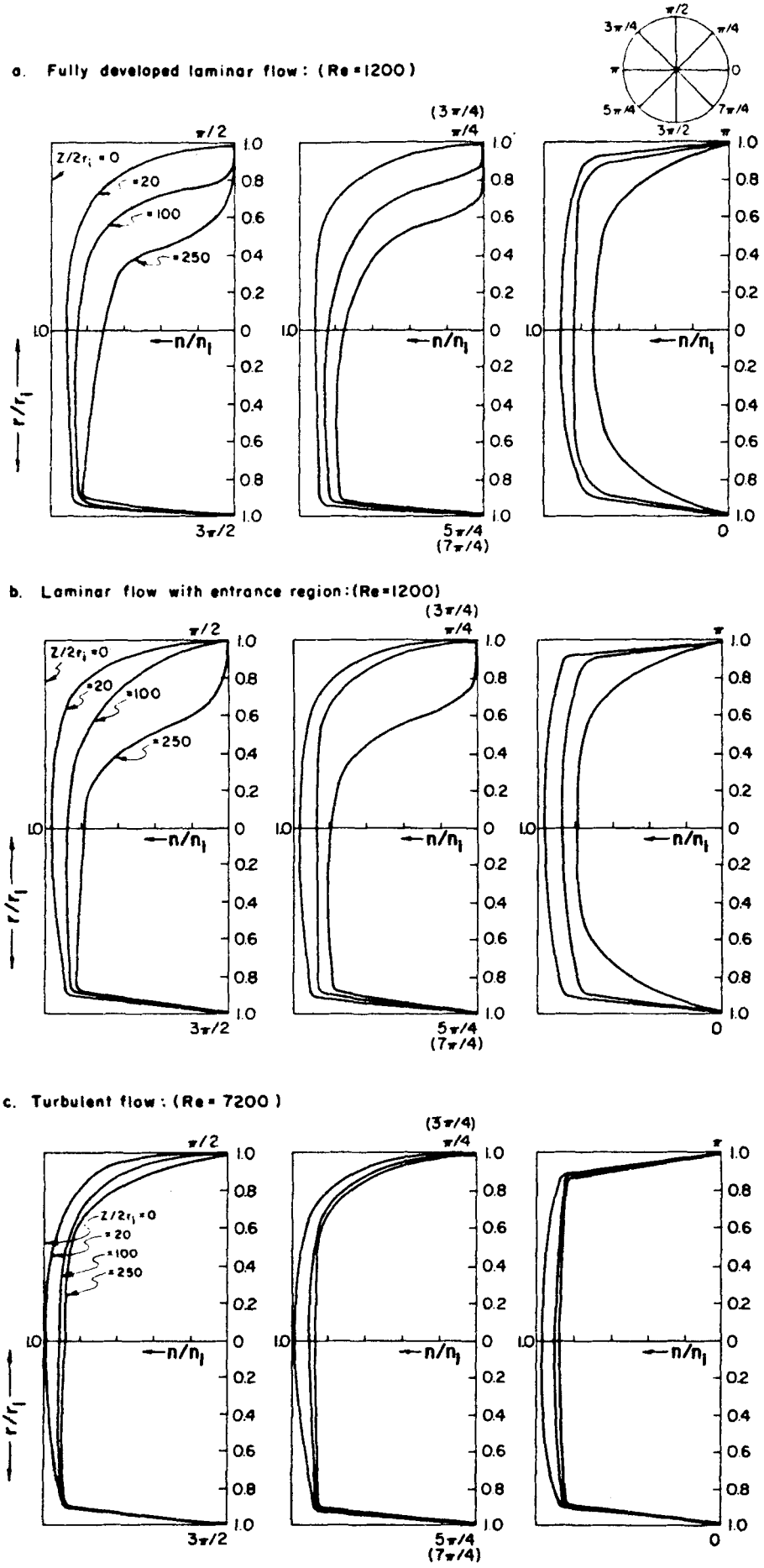

Figure 7. Particle concentration profile: $d = 2.6\ \mu m$, horizontal pipe.

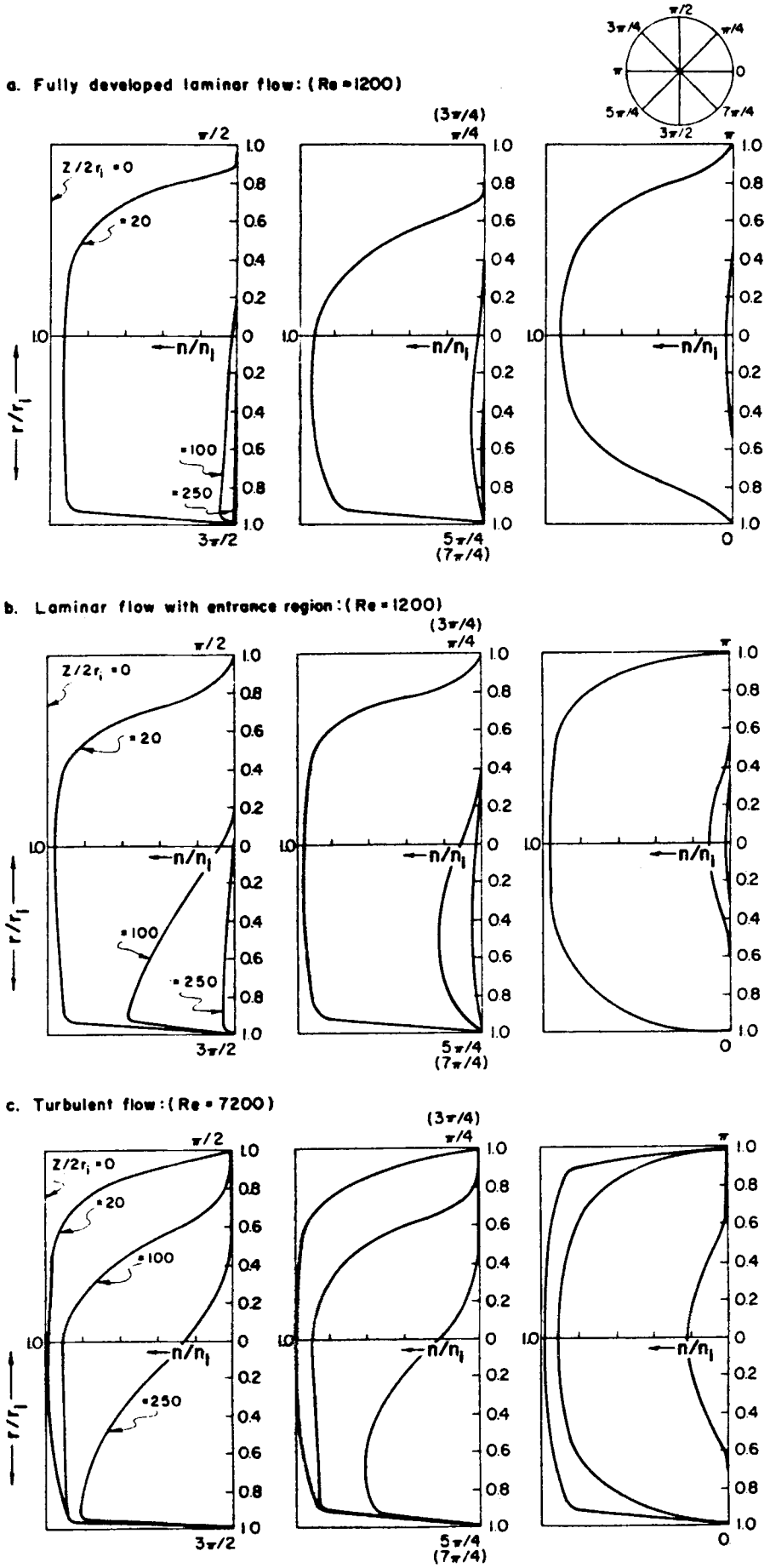

Figure 8. Particle concentration profile: $d = 12\ \mu m$, horizontal pipe.

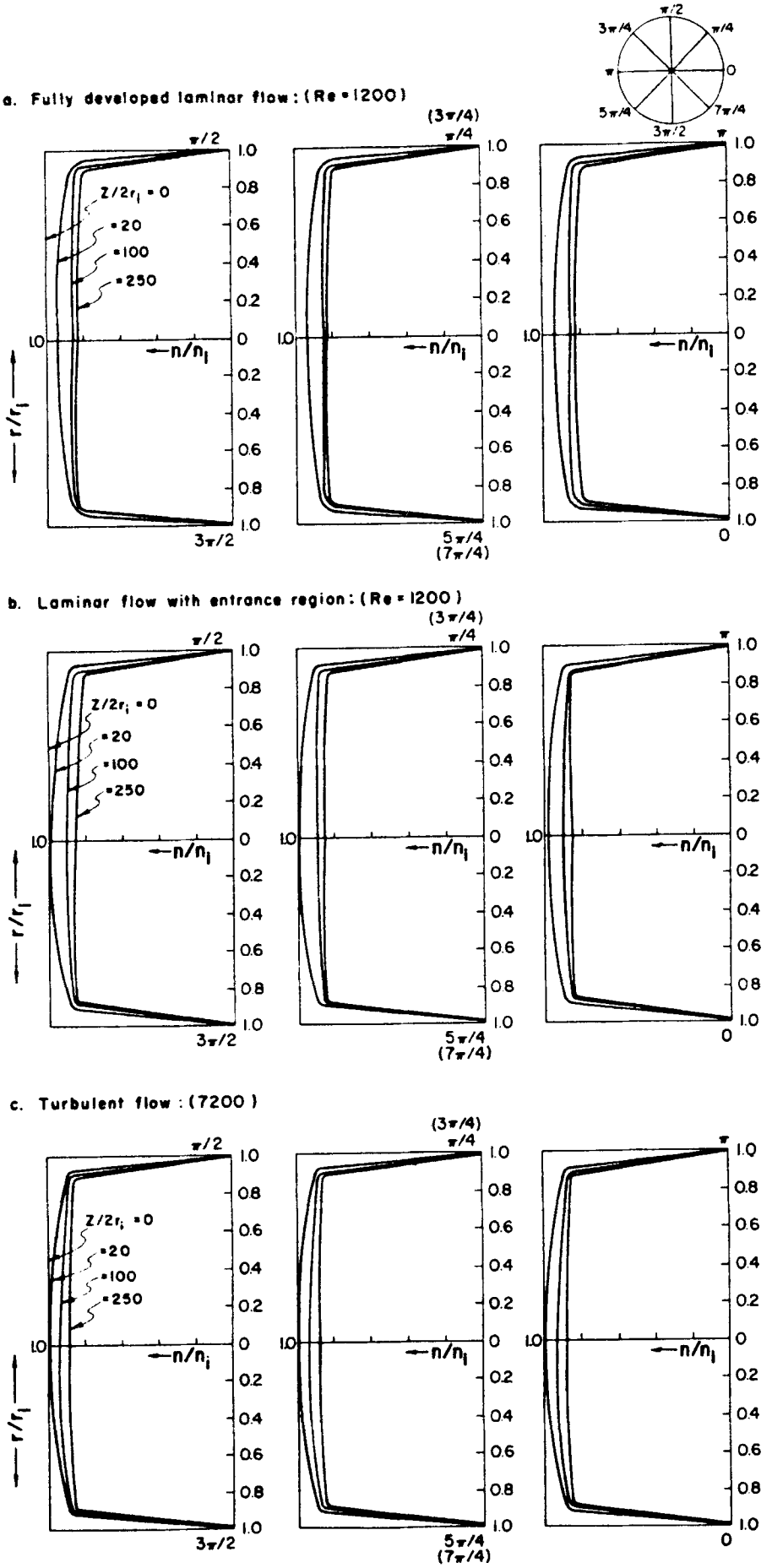

Figure 9. Particle concentration profile: $d = 0.2\ \mu m$, horizontal pipe.

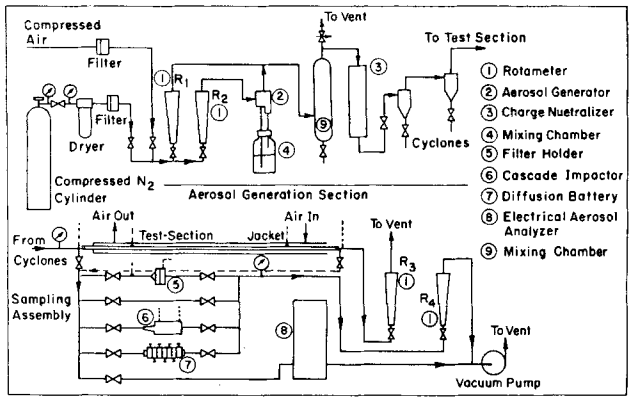

Figure 10. Schematic diagram of the experimental setup.

Comparison of Figures 11b and 11c illustrates the effect of flow rate. It appears that flow rate has very little effect on aerosol size distribution but there is an observable difference in aerosol penetration; e.g., the fractional penetration obtained at flow rate of 333.3×10^{-6} m^3/s is greater than that obtained at 83.3×10^{-6} m^3/s. This is explained by the fact that at higher stream flow rates, the magnitudes of diffusive, settling, and thermophoretic effects, which contribute to the particle deposition at the wall, are smaller in comparison with convective transport in the axial direction.

Temperature gradients are responsible for thermophoretic forces and for condensation and nucleation processes. Comparison of data in Figures 11b and 11d, which were obtained under conditions differing only in the magnitude of temperature gradients, shows that at higher temperature gradients the deposition is greater, but there is no observable change in size distribution. Since the effect of condensation and nucleation processes is mainly to alter the size distribution, the results indicate that these processes have very little effect on particle dynamics under the experimental conditions. On the other hand, thermophoresis seems to have an important effect on particle deposition.

In all cases however, the experimental and theoretical size distributions show good agreement. The comparison of fractional mass penetration values obtained experimentally and calculated theoretically show a satisfactory agreement. At higher flow rates, both indicate less deposition and hence greater penetration. Under high temperature gradients, both point to a greater deposition and less penetration. The small differences could be accounted for by errors in experimental measurements. The agreement between theoretical predictions and experimental results proves the applicability of the theoretical model. In the numerical computations, the developing velocity profile in the test section entrance region was indeed taken into account.

In order to find the relative importance of the thermophoresis, sedimentation, and Brownian diffusion under experimental conditions, fractional penetration due to each process was calculated numerically assuming the other two to be absent. Results of this exercise for a sample experimental observation are presented in Table 2. It can be seen that wall deposition due to Brownian diffusion and sedimentation is almost negligible at the experimental conditions. The 5% deposition is almost entirely due to thermophoresis. This illustrates the importance of temperature gradients and supports the earlier conclusions.

TABLE 2. RELATIVE MAGNITUDES OF THERMOPHORESIS, SEDIMENTATION, AND BROWNIAN DIFFUSION

Propylene glycol aerosol; Inlet temperature = 373 K; Wall temperature = 298 K; Atomization: dilution = 1:0; Flow rate = 136.7×10^{-6} m^3/s (std. cond.)

Particle Dia. (μm)	Fractional Penetration: Brownian Diff.	Sedimentation	Thermophoresis
0.200	0.99949	0.99942	0.95757
0.280	0.99972	0.99889	0.95407
0.370	0.99980	0.99813	0.95231
0.500	0.99998	0.99689	0.95163
0.620	1.00000	0.99535	0.95171
0.750	0.99994	0.99339	0.95218
1.000	1.00005	0.98895	0.95331
Overall fractional no. penetration	0.99968	0.99863	0.95462
Overall fractional mass penetration	0.99985	0.99682	0.95283

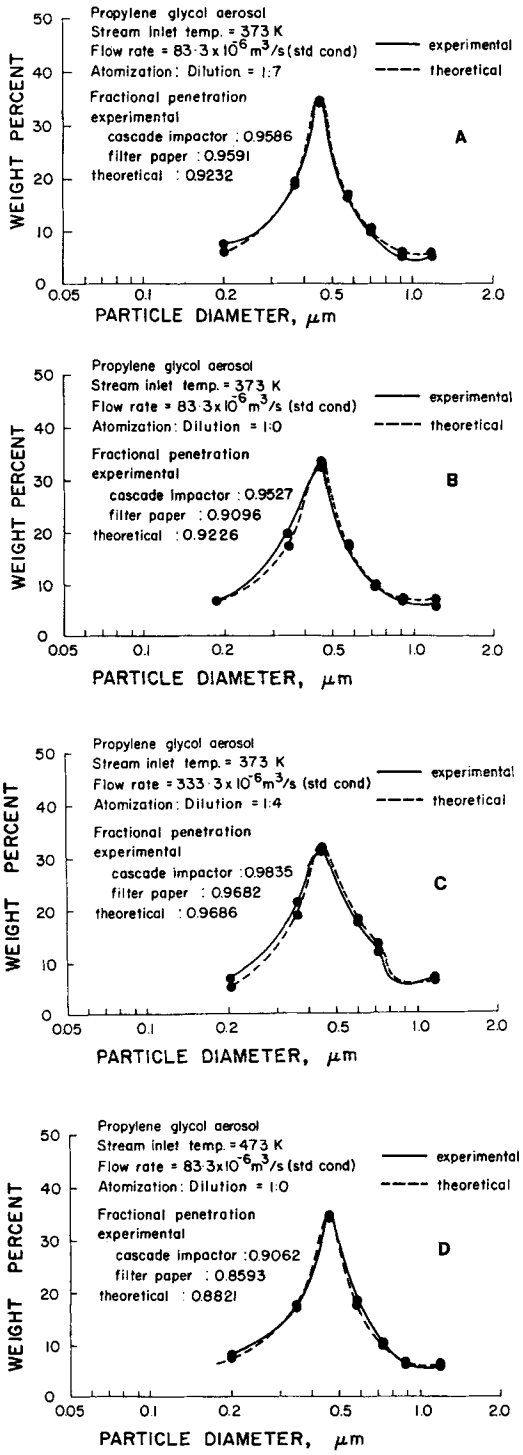

Figure 11. Aerosol size distribution at test section outlet.

ACKNOWLEDGMENT

This research work was supported by the U.S. Department of Energy under Contract #DE-AC21-80MC14374,M003. The

contribution by P. D. Nguyen to the experimental work is gratefully acknowledged.

NOTATION

a_c = accommodation coefficient for gas molecules on particle surface
C = specific heat, J/kg·K
C_d = Cunningham correction factor
D_v = diffusivity of vapor, m^2/s
D_p = particle diffusivity in the gas, m^2/s
d = particle diameter, m
d_o = diameter of nucleus, m
G_o = free energy, J
g = gravitational acceleration, m/s^2
I = condensation growth rate, m/s
K = thermal conductivity of the gas, W/m·K
K_p = thermal conductivity of the particle, W/m·K
Kn = Knudsen number
k = Boltzmann constant
M = gas molar mass, kg/kmol
M_p = particle molar mass, kg/kmol
m = mass of a molecule, kg
N_o = overall particle number density at the inlet, No./m^3
n = number density of particles, No./m^3
$\dot{n}$ = rate of change in number density, No./m^3·s
n_i = number density of particles at the inlet, No./m^3
R_g = universal gas constant, J/mol·K
p = partial pressure of the condensable vapor, N/m^2
p' = vapor pressure, N/m^2
q = wall heat flux, W/m^2
r = radial coordinate, m
r_t = pipe radius, m
S_o = rate of formation of nuclei, No./m^3·s
T = temperature, K
T_i = inlet temperature, K
T_w = wall temperature, K
$\bar{u}$ = gas mean molecular velocity, m/s
v_g = terminal settling velocity, m/s
V_L = molar volume of liquid, m^3
v_{Tr} = radial thermophoretic velocity, m/s
v_{Tz} = axial thermophoretic velocity, m/s
v_z = axial stream velocity, m/s
$\bar{v}_z$ = average axial stream velocity, m/s
z = axial coordinate, m

Greek Letters

α = thermal diffusivity, m^2/s
β = coagulation coefficient, m^3/s
∇ = gradient, m^{-1}
δ = Dirac delta function
θ = angular coordinate
λ = gas mean free path, m
μ = gas viscosity, kg/m·s
ρ = gas density, kg/m^3
ρ_p = particle density, kg/m^3
ρ_v = vapor density, kg/m^3
σ = surface tension, N/m

LITERATURE CITED

Berezhnoi, V. M., and V. V. Kirichenko, *Atom. Energ.*, **17**, 300 (1964).
Crump, J. G., and J. H. Seinfeld, "Aerosol Behavior in a Continuous Stirred Tank Reactor," *AIChE J.*, **26**, 610 (1980).
Damle, A. S., and R. Mahalingam, "Behavior of Polydisperse Aerosols Inside a Closed Sphere," *J. Colloid & Interface Sci.*, 87(1), 242 (1982).
DeMarcus, W., and J. W. Thomas, "Theory of Diffusion Battery," ORNL-1413, Oak Ridge National Laboratory, Oak Ridge, TN (1952).
Gelbard, F., and J. H. Seinfeld, "Exact Solution of the General Dynamic Equation for Aerosol Growth by Condensation," *J. Colloid & Interface Sci.*, **68**, 173 (1979).
Gormley, P. G., and M. Kennedy, *Proc. R. Irish Acad.*, **52**, 163 (1949).
Hidy, G. M., and J. R. Brock, *The Dynamics of Aerocolloidal Systems*, Pergamon Press, Oxford, UK (1970).
Hsu, C. J., "An Exact Mathematical Solution for Entrance Region Laminar Heat Transfer with Axial Conduction," *Appl. Sci. Res.*, **17**, 359 (1967).
Langhaar, H. L., "Steady Flow in the Transition Length of a Straight Tube," *Trans. ASME*, **64**, A55 (1942).
Moo-Young, M., and K. Yamaguchi, "Analysis of Thermophoretic Deposition of Aerosol Particles from Laminar-Flow Gas Streams," *Chem. Eng. Sci.*, **30**, 1,291 (1975).
Nadkarni, A. R., "Aerosol Dynamics in Temperature and Concentration Gradient Fields, Applied to Coal Gasification," M.S. Thesis, Washington State Univ. (1982).
Nguyen, P., and R. Mahalingam, "Temperature and Concentration Effects on Dynamic Behavior of Fine Particles in a Continuous Stirred Tank Reactor," Paper #F-1, *Proc. Int. Symp. Recent Adv. Particulate Sci. & Tech.*, Madras, India (Dec., 1982).
Pilat, M. J., and A. Prem, "Calculated Particle Collection Efficiencies of Single Droplets Including Inertial Impaction, Brownian Diffusion, Diffusiophoresis and Thermophoresis," *Atmos. Environ.*, **10**, 13 (1976).
Tan, C. W., and C. J. Hsu, "Diffusion of Aerosols in Laminar Flow in a Cylindrical Tube," *J. Aerosol Sci.*, **2**, 117 (1971).

Manuscript received June 1, 1983; revision received Feb. 14, 1984, and accepted Mar. 1.